Strong Enhancement of the Spin Hall Effect by Spin Fluctuations near the Curie Point of Fe_xPt_{1-x} Alloys

Yongxi Ou,[1,*] D. C. Ralph,[1,2] and R. A. Buhrman[1,†]
[1]Cornell University, Ithaca, New York 14853, USA
[2]Kavli Institute at Cornell, Ithaca, New York 14853, USA

(Received 1 October 2017; revised manuscript received 19 November 2017; published 1 March 2018)

Robust spin Hall effects (SHE) have recently been observed in nonmagnetic heavy metal systems with strong spin-orbit interactions. These SHE are either attributed to an intrinsic band-structure effect or to extrinsic spin-dependent scattering from impurities, namely, side jump or skew scattering. Here we report on an extraordinarily strong spin Hall effect, attributable to spin fluctuations, in ferromagnetic Fe_xPt_{1-x} alloys near their Curie point, tunable with x. This results in a dampinglike spin-orbit torque being exerted on an adjacent ferromagnetic layer that is strongly temperature dependent in this transition region, with a peak value that indicates a lower bound 0.34 ± 0.02 for the peak spin Hall ratio within the FePt. We also observe a pronounced peak in the effective spin-mixing conductance of the FM/FePt interface, and determine the spin diffusion length in these Fe_xPt_{1-x} alloys. These results establish new opportunities for fundamental studies of spin dynamics and transport in ferromagnetic systems with strong spin fluctuations, and a new pathway for efficiently generating strong spin currents for applications.

DOI: 10.1103/PhysRevLett.120.097203

The manipulation of the magnetization in ferromagnetic (FM) nanostructures with pure spin current densities J_s has become a primary tool in spintronics since the demonstrations of nanomagnet switching driven by large spin orbit torques (SOT) originating from the spin Hall effect (SHE) [1–4] in an adjacent heavy metal carrying a longitudinal electrical current density J_e. Most SOT efforts so far have focused on the utilization of large *intrinsic* spin Hall ratios, $\theta_{SH} \equiv (2e/\hbar)J_s/J_e$, for certain heavy metals that are compatible with the requirements of a successful spintronics technology [5–9]. An alternative approach to enhance θ_{SH} is to introduce dopants into a metallic system whereby strong spin-orbit interactions can strengthen the spin Hall effect, either by enhanced *extrinsic* spin-dependent skew or side-jump scattering, or by the intrinsic effect through a beneficial modification of the electronic band structure at the Fermi level [10]. Typically the dopant has been a heavy element without a strong magnetic moment, e.g., Ir, Bi, Au [11–14], and the resulting enhancement, usually attributed to skew scattering, has been measured by the inverse spin Hall effect or by a nonlocal spin accumulation technique. Recently Wei *et al.* [15] have reported a moderate, but notable, temperature-dependent enhancement of the inverse spin Hall effect in dilute NiPd alloys, attributed to spin-fluctuation-enhanced skew scattering by the Ni ions in the vicinity of the ferromagnetic transition. We note that NiPd is one of a class of ferromagnetic alloys that have long been known to exhibit giant magnetic moments per ferromagnetic solute, particularly in the dilute limit [16]. Reference [15] provides strong motivation for examining the direct SHE in other ferromagnetic alloys in which there can be a stronger spin-orbit interaction between the conduction electrons and the ferromagnetic component. Here we demonstrate that for Fe-doped Pt alloys, Fe_xPt_{1-x}, the effective spin Hall angle as measured directly from the dampinglike torque exerted on an adjacent ferromagnetic layer is increased by more than a factor of 3 in the vicinity of its Curie temperature T_c in comparison to the already-substantial value it has well above T_c, and at its peak has a value at least comparable to that of beta-W [5], and with a much lower electrical resistivity.

Fe_xPt_{1-x} alloys are well known for their unusually robust magnetic anisotropy properties arising from the strong conduction electron spin-orbit interaction with the Fe orbital moment [17,18], and also for the dependence of the magnetic state on the chemical order. For example, well-ordered $Fe_{0.25}Pt_{0.75}$ exhibits antiferromagnetism, while chemically disordered $Fe_{0.25}Pt_{0.75}$ is ferromagnetic [19,20]. Ferromagnetic Fe_xPt_{1-x} films also exhibit quite large anomalous Hall effects (AHE) [21–23], which suggests that Fe_xPt_{1-x} can be a promising material for the generation of spin currents by the extrinsic SHE.

To investigate this possibility we prepared multilayers containing two different sets of Fe_xPt_{1-x} thin films made by codeposition at room temperature via dc magnetron sputtering; in one case the nominal composition was $Fe_{0.15}Pt_{0.85}$ and in the other $Fe_{0.25}Pt_{0.75}$. Multilayer stacks consisting of substrate/Ta/IrMn/Fe_xPt_{1-x}/MgO/Ta were used for thin film characterization and substrate/Ta/IrMn/Fe_xPt_{1-x}/Hf/FeCoB/Hf/MgO/Ta stacks were used for the SOT measurements. These samples were prepared by direct current (dc) sputtering (with rf magnetron sputtering for the MgO

layer) in a deposition chamber with a base pressure $<5 \times 10^{-8}$ Torr. The dc sputtering condition was 2 mTorr Ar pressure. The Fe_xPt_{1-x} alloy was grown by cosputtering from two pure sputtering targets (i.e., Fe and Pt targets). All samples in this work had a Ta(1 nm) seed layer to provide a smooth base layer and a Ta(1 nm) top layer to provide an oxidized protection layer for the stack. All samples were annealed in an in-plane magnetic field (2000 Oe) in a vacuum furnace at 300 °C for 1 h to enhance the PMA. For measurements of the AHE and SOT, Hall bar devices with lateral dimensions of 5×60 μm^2 were patterned via photolithography and ion milling [see the sample schematic in Fig. 1(d)].

We performed x-ray diffraction (XRD) measurements on two multilayer samples with the layer structures $IrMn_3(10)/Fe_{0.15}Pt_{0.85}(10)/MgO$ and $IrMn_3(10)/Fe_{0.25}Pt_{0.75}(10)/MgO$ (the number in parentheses is the thickness in nanometers). The $IrMn_3$ layer was included to provide antiferromagnetic pinning of the Fe_xPt_{1-x} layers when cooled to well below their Curie points for research that will be presented elsewhere; the Fe_xPt_{1-x} layers are thick enough that in the experiments to be considered below the $IrMn_3$ does not contribute any significant SOT on the free magnetic layer. We show in Fig. 1(a) the (111) XRD peaks for the $Fe_{0.15}Pt_{0.85}$ and the $Fe_{0.25}Pt_{0.75}$ samples, and also for separate 10 nm Pt, $Fe_{0.50}Pt_{0.50}$, and IrMn films for comparison. The (111) peak is reasonably narrow, shifting to higher 2θ angle as the Fe content increases, indicating a decrease in the unit cell size with increased Fe content. As expected from the use of room temperature deposition there was no evidence of a (110) peak in the XRD of these samples that would indicate significant chemical order [24] [The small peak at $2\theta \approx 41°$ in Fig. 1(a) is due to the $IrMn_3$ base layer]. Finally, as expected for a disordered metal the resistivity of the films was only weakly temperature dependent, decreasing by less than 10% from room temperature to 160 K, indicating the dominance of impurity scattering. The resistivity of the films did vary with Fe content, from $\rho_{Pt}(10) \approx 15\ \mu\Omega \cdot cm$ to $\rho_{Fe_{0.15}Pt_{0.85}}(10) \approx 55\ \mu\Omega \cdot cm$ to $\rho_{Fe_{0.25}Pt_{0.75}}(10) \approx 75\ \mu\Omega \cdot cm$, indicating an increased electron scattering rate with increased Fe content.

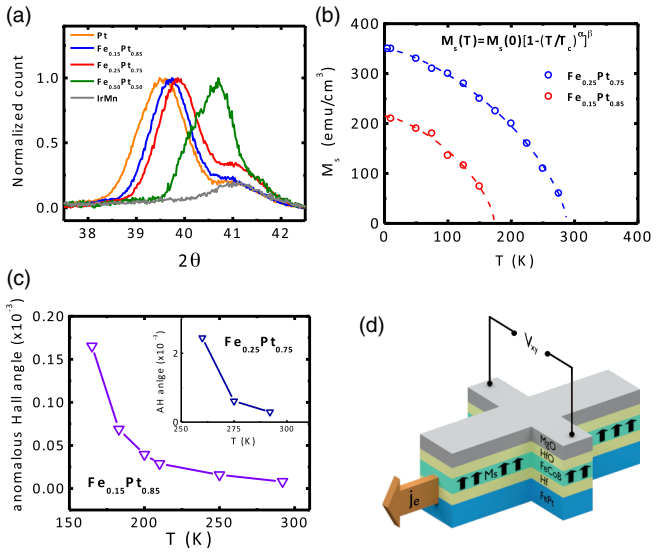

FIG. 1. (a) XRD measurements on the samples $IrMn_3(10)/F_{0.50}Pt_{0.50}(10)/MgO$, $IrMn_3(10)/Fe_{0.25}Pt_{0.75}(10)/MgO$, and $IrMn_3(10)/Fe_{0.15}Pt_{0.85}(10)/MgO$, and two control samples $IrMn_3(10)/Pt(1)/MgO$ and $IrMn_3(10)/Pt(8)/MgO$. (b) Temperature dependent VSM measurements on the samples $IrMn_3(10)/Fe_{0.25}Pt_{0.75}(10)/MgO$ and $IrMn_3(10)/Fe_{0.15}Pt_{0.85}(10)/MgO$. The dashed lines are fits to the empirical equation $M_s(T) = M_s(0)[1 - (T/T_c)^{\alpha}]^{\beta}$. (c) Temperature dependence of the anomalous Hall angle of the samples $IrMn_3(10)/Fe_{0.15}Pt_{0.85}(10)/MgO$ (main) and $IrMn_3(10)/Fe_{0.25}Pt_{0.75}(10)/MgO$ (inset). (d) Schematic of the Hall bar device.

To further confirm the chemical disorder and the ferromagnetic character of these alloys we made temperature-dependent vibrating sample magnetometry (VSM) measurements of the samples [Fig. 1(b)]. Both $Fe_{0.15}Pt_{0.85}$ and $Fe_{0.25}Pt_{0.75}$ were found to be ferromagnetic at sufficiently low temperature, with fits of the spontaneous magnetization $M_s(T)$ to the empirical function $M_s(T) = M_s(0)[1 - (T/T_c)^{\alpha}]^{\beta}$ [25] yielding a Curie temperature of $T_c \approx 174$ K for the $Fe_{0.15}Pt_{0.85}$ sample and $T_c \approx 288$ K for the $Fe_{0.25}Pt_{0.75}$ sample.

In Fig. 1(c) we show the temperature dependence of the "anomalous Hall angle" $=\rho_{xy}/\rho_{xx}$ of the $Fe_{0.15}Pt_{0.85}(10)$ and $Fe_{0.25}Pt_{0.75}(10)$ samples as measured in a magnetic field $H_z = 2$ kOe applied perpendicular to the plane of the film. (Here ρ_{xx} is the resistivity in the direction of current flow and ρ_{xy} is the transverse Hall resistivity). As can be seen in the $Fe_{0.15}Pt_{0.85}(10)$ sample, there is a significant AHE at high temperature that increases gradually as the temperature is decreased toward 200 K and then increases more rapidly as the magnetization in the film develops as T decreases below T_c, qualitatively as would be expected for the case of strong skew scattering from the Fe ions. In the inset of Fig. 1(c), there is a similar temperature dependence trend for the $Fe_{0.25}Pt_{0.75}(10)$ sample below its Curie temperature. In the AHE what is detected is the charge flow in the direction perpendicular to the plane defined by the bias current direction $\boldsymbol{y}$ and the direction of the internal magnetic field $\boldsymbol{z}$. This transverse charge flow is accompanied by a diffusive spin current arising from the spin-dependent scattering. The resulting V_{AHE}, or, equivalently, ρ_{xy}, scales for the extrinsic case with the rate of skew scattering, but it also depends on the strength of the internal magnetization of the material and its spin dependent charge transport properties. This makes it challenging to quantify the underlying spin flow based only on AHE measurements.

To achieve better quantitative measurements of the spin currents produced by an electrical current in the FePt alloys we employed the harmonic response SOT technique [26,27], whereby we measured the magnetic deflection of

an adjacent, perpendicularly magnetized ferromagnetic thin film that occurs as the result of the spin torque arising from the absorption of the transverse polarized component of the spin current emanating from the spin source, the FePt alloys in this case. Such measurements of SOT effective fields usually only set a lower bound on θ_{SH} due to the expected less than perfect spin transparency of the interface between the spin source and spin sink [28,29].

For the harmonic response SOT measurements we fabricated two sets of FePt-based multilayer samples: $IrMn_3(10)/Fe_{0.15}Pt_{0.85}(10)/Hf(1)/FeCoB(1)/Hf(0.35)/MgO$ (A), and $IrMn_3(10)/Fe_{0.25}Pt_{0.75}(10)/Hf(0.8)/FeCoB(1)/Hf(0.35)/MgO$ (B), where FeCoB represents $Fe_{60}Co_{20}B_{20}$. The amorphous Hf insertion layer [1 and 0.8 nm for (A) and (B), respectively] between the FePt and the FeCoB was employed to counter the detrimental effect of the fcc crystal structure of the FePt on obtaining perpendicular magnetic anisotropy (PMA) in the thin FeCoB layer, while the very thin (0.35 nm) Hf insertion layer between the FeCoB and the MgO enhanced the interfacial magnetic anisotropy energy density, strengthening the PMA [30].

In Fig. 2(a), we show the response of the anomalous Hall resistance of one of the $Fe_{0.15}Pt_{0.85}$ heterostructure Hall bars (sample A) to an applied out-of-plane field H_z at different temperatures between 300 and 140 K. The sharp field-induced switching events, with an increasing coercivity upon decreasing temperature, are from the PMA FeCoB layer. When the temperature is lower than the Curie temperature of $Fe_{0.15}Pt_{0.85}$ there is also a quasilinear background evident for H_z greater than the coercive fields that is much larger than can be expected from the ordinary Hall effect, and instead is due to the AHE of the in-plane magnetized FePt layer. The AHE resistance for sample (B) is similar [31].

We determined the dampinglike (DL) and fieldlike (FL) effective fields (ΔH_{DL} and, ΔH_{FL} respectively) arising from the SOT by measuring the first and second harmonic transverse Hall signals V_ω and $V_{2\omega}$ [27], from which we obtain $\Delta H_{L(T)} = -2(\partial V_{2\omega}/\partial H_{L(T)})/(\partial^2 V_\omega/\partial H^2_{L(T)})$ and, hence, $\Delta H_{DL} = (\Delta H_L + 2\delta\Delta H_T)/(1-4\delta^2)$ and $\Delta H_{FL} = (\Delta H_T + 2\delta\Delta H_L)/(1-4\delta^2)$. Here, $H_{L(T)}$ is the external bias field applied parallel to (transverse to) the current direction and δ is the ratio of the planar Hall resistance to the anomalous Hall resistance [26,27].

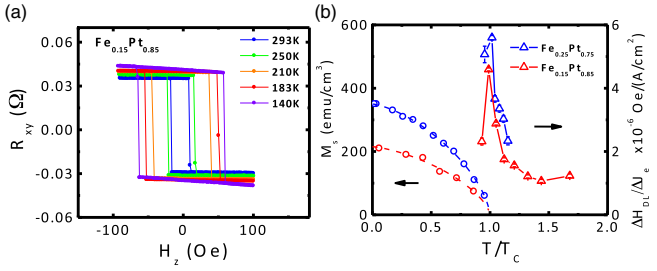

FIG. 2. (a) Temperature dependent AHE resistance of sample (A) $Fe_{0.15}Pt_{0.85}$. (b) Dampinglike effective fields of sample (A) $Fe_{0.15}Pt_{0.85}$ and (B) $Fe_{0.25}Pt_{0.75}$ as a function of normalized temperature T/T_c. Their temperature dependent magnetizations are also plotted here for comparison.

In Fig. 2(b) we show the temperature dependences of the DL effective fields for both sample (A) and sample (B), plotted as a function of T/T_c, with T_c determined from the fits to the magnetization of the samples [Fig. 1(b)] (See Supplemental Material [31] for discussion of the FL SOT behavior of these samples). For sample (A) ($Fe_{0.15}Pt_{0.85}$) the measurement is from room temperature 293 to $T = 160$ K, and for sample (B) ($Fe_{0.25}Pt_{0.75}$) from 330 to 275 K. For sample (A) for which we have measurements starting around 100° K above T_c, we see that the DL effective field per current density $\Delta H_{DL}/\Delta J_e$ is more or less constant until $T/T_c \approx 1.44$ (250 K), below which it increases, at first gradually, then very rapidly reaching a peak near T_c (172 K) more than 3 times its 293 K value. This behavior is dramatically different from that of the DL torque found with conventional heavy metal systems [32,33]. Below this peak $\Delta H_{DL}/\Delta J_e$ then drops off even more quickly until below $T/T_c = 0.92$ (160 K) the observable development of spin torque from the PMA FeCoB on the emerging strong ferromagnetism of the in-plane polarized $Fe_{0.15}Pt_{0.85}$ makes further quantitative harmonic response measurements untenable (see Supplemental Material [31] for more information).

As also shown in Fig. 2(b), the behavior of sample (B) over the same scaled temperature range above and below T_c, is quite similar, with the peak value of $\Delta H_{DL}/\Delta J_e$ being less than 20% different than that of sample (A), and even less if we take into account the spin attenuation effect of the different Hf spacer thickness (1 nm for sample A and 0.8 nm for sample B) where Hf has a spin diffusion length of approximately 1 nm [34]. This close similarity in the values of the peak antidamping spin torque is observed despite the 35% difference in resistivity, and 67% difference in Fe concentration. This is consistent with skew scattering being the dominant spin Hall effect in these materials, at least in the ferromagnetic transition region, but more study will be needed to confirm that attribution.

Some years ago Kondo [35] developed a theory for the scattering of conduction electrons by localized orbital moments to explain an anomaly in the magnetoresistance and AHE of ferromagnetic Ni and Fe near their Curie points [36], with Kondo attributing the anomaly to increasingly stronger spin fluctuations as $T \to T_c$ from below. Recently Gu *et al.* [37] extended this theory to explain results by Wei *et al.* [15] on inverse spin Hall effect (ISHE) measurements of NiPd alloys near their T_c, including the effect of correlations between neighboring localized moments. We surmise that spin fluctuations are also the origin of the strong peak in the SOT torque (spin current) that we observe with the FePt alloys, although our results, in addition to being a direct measure of the J_s generated by the spin Hall effect,

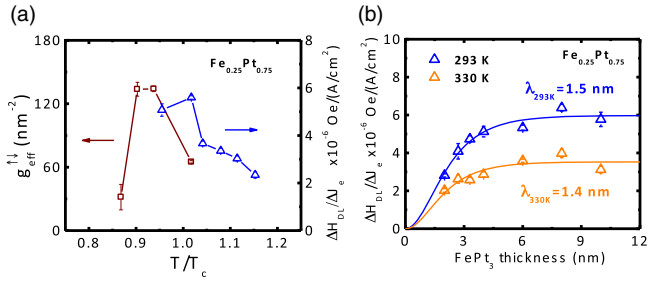

FIG. 3. (a) The effective spin mixing conductance of an in-plane magnetized $Fe_{0.25}Pt_{0.75}(10)/Hf(0.25)/FeCoB(7.3)$ sample as determined by a flip-chip FMR measurement of the damping parameter for the FeCoB resonance. The temperature dependence of the DL effective field of sample (B) is also plotted here for comparison. (b) Spin diffusion length measurement of the samples $Fe_{0.25}Pt_{0.75}(t)/Hf(0.8)/FeCoB(1)$.

differ from the earlier work by the strength of the effect, which we attribute to the exceptionally strong spin-orbit interaction in the Fe-Pt system. Our results are also distinctive in that the peak in the SOT effective field (emitted spin current) is followed by a sharp decline with decreasing temperature that we attribute to the effect of the internal exchange field in the FePt that develops as T is lowered below T_c, which, once well established, acts to quickly dephase a spin current that is polarized in a direction not collinear with the internal magnetization [23].

If spin fluctuations are indeed the origin of the enhanced SHE in the FePt alloys near T_c, then it is predicted [38] that there should also be an enhancement of the effective interfacial spin-mixing conductance $g^{\uparrow\downarrow}_{\text{eff}}$ between the FeCoB and FePt alloy in the vicinity of the latter's Curie point, as has been recently observed with *antiferromagnetic* spin sinks near their Néel point by inverse spin Hall measurements [39] and spin pumping [40]. In the latter case the interfacial enhancement of damping $\Delta\alpha \equiv \alpha(t_{\text{FM}}) - \alpha_0$, where α_0 is the Gilbert damping parameter for the bulk FM material, can be related to $g^{\uparrow\downarrow}_{\text{eff}}$ by $g^{\uparrow\downarrow}_{\text{eff}} = 4\pi M_s t_{\text{FeCoB}} \Delta\alpha/(\gamma\hbar)$ [41]. We do indeed observe a pronounced peak in magnetic damping of the FeCoB layer in our samples as they are cooled through the T_c of the FePt. In Fig. 3(a) we show the effective spin mixing conductance, $g^{\uparrow\downarrow}_{\text{eff}}$ as determined by resonant linewidth measurements made by flip-chip field-modulated FMR, on a $Fe_{0.25}Pt_{0.75}(10)/Hf(0.25)/FeCoB(7.3)/MgO$ sample (See Supplemental Material [31] for details of measurements). As can be seen $g^{\uparrow\downarrow}_{\text{eff}}$ increases rapidly as T moves below T_c, and then drops abruptly by more than a factor of 3 to a value ($\approx 30\text{nm}^{-2}$) much closer to that expected for a typical FM/Pt interface [29]. The temperature-dependent behavior observed here is distinctly different from the temperature-insensitive $g^{\uparrow\downarrow}_{\text{eff}}$ in Pt/ferromagnet bilayer systems [42]. Note that the peak in $g^{\uparrow\downarrow}_{\text{eff}}$ does not occur simultaneously with the peak in $\Delta H_{\text{DL}}/\Delta J_e$ which indicates that the latter's peak is not just due to an enhanced $g^{\uparrow\downarrow}_{\text{eff}}$.

To better quantify the peak strength of SHE in the FePt alloys and to account for the spin current attenuation in the Hf spacer layer, we prepared another $Fe_{0.25}Pt_{0.75}$ heterostructure, $IrMn_3(10)/Fe_{0.25}Pt_{0.75}(10)/Hf(0.5)/FeCoB(0.9)/Hf(0.35)/MgO$, i.e., with a thinner (0.5 nm) Hf spacer layer. In Table I we compare the peak $\Delta H_{\text{DL}}/\Delta J_e$ value that we obtained with a Hall bar measurement of this sample to that previously measured [33] for a $Pt(4)/Hf(0.5)/FeCoB(1)/MgO$ sample at 293 K (room temperature). Assuming the same spin current attenuation in both cases from the 0.5 nm Hf/FeCoB interface, this indicates that the peak spin Hall effect in the $Fe_{0.25}Pt_{0.75}$ is approximately 5.5x larger than in Pt(4). More quantitatively, with the torque-field relation $\xi_{\text{DL}} = (2e/\hbar) M_s t_{\text{FeCoB}} (\Delta H_{\text{DL}}/\Delta J_e)$ [29], we can calculate the DL spin torque efficiency $\xi_{\text{DL}} = 0.34 \pm 0.02$ for the sample $Fe_{0.25}Pt_{0.75}(10)/Hf(0.5)/FeCoB(1)$. Considering the attenuation of the spin current as it passes through the 0.5 nm of Hf, and the likely less than ideal spin transparency of the Hf/FeCoB interface, this only sets the *lower bound* for the peak spin Hall ratio of the $Fe_{0.25}Pt_{0.75}$ material as ≥ 0.34.

Another key parameter for understanding and optimizing the effectiveness of SOTs arising from the SHE is the spin diffusion length λ_s within the material. We obtained a measure of λ_s by producing a series of PMA samples without the IrMn layer $Fe_{0.25}Pt_{0.75}(t_{\text{FePt}})/Hf(0.8)/FeCoB(1)/Hf(0.35)/MgO/Ta(1)$, where the thickness t_{FePt} of the FePt alloy was varied from 2 to 10 nm. The measured dampinglike effective fields for these samples are plotted in Fig. 3(b) as a function of t_{FePt} for two different temperatures 293 and 330 K, i.e., in the near vicinity of T_c and somewhat above it. The solid lines are a fit of the function $\Delta H_{\text{DL}}(t_{\text{FePt}})/\Delta J_e = [\Delta H_{\text{DL}}(\infty)/\Delta J_e][1 - \text{sech}(t_{\text{FePt}}/\lambda_s)]$ [43] to the data. The results at the two temperatures are quite similar, with $\lambda_s \approx 1.5$ nm.

TABLE I. Comparison of the dampinglike effective fields as measured at 293 K for two $Fe_{0.25}Pt_{0.75}$/Hf/FeCoB samples and a Pt/Hf/FeCoB sample.

Sample	$Fe_{0.25}Pt_{0.75}(10)/Hf(0.8)/FeCoB(1)$	$Fe_{0.25}Pt_{0.75}(10)/Hf(0.5)/FeCoB(1)$	$Pt(4)/Hf(0.5)/FeCoB(1)$
DL effective field$\times 10^{-6}$ Oe/(A/cm^2)	5.6	12.2	2.3
Reference	This work	This work	Ou *et al.* [33]

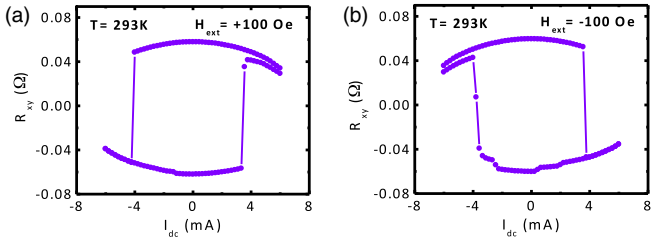

FIG. 4. Current-induced magnetization switching of sample (B) $IrMn_3(10)/Fe_{0.25}Pt_{0.75}(10)/Hf(0.8)/FeCoB(1)/Hf(0.35)/MgO$ at room temperature under an external magnetic field along the current direction.

We further confirm the strength of the SHE in the FePt alloys with current-induced switching measurements. In Fig. 4 we show the switching behavior of sample (B) as measured at 293 K, in close vicinity to T_c. The direction of current-induced switching is reversed upon changing the sign of a small in-plane applied magnetic field, in a way that is characteristic of antidamping torque SHE switching [44]. The switching current density for this case was $\approx 6 \times 10^6$ A/cm^2.

In summary, we have studied the spin-orbit torques resulting from the SHE in chemically disordered FePt alloys, above and through their ferromagnetic transition points T_c. The SOTs exerted by these materials on an adjacent FeCoB thin film exhibit a striking temperature dependence in which the DL SOT displays a strong maximum in the vicinity of T_c. We attribute this pronounced SOT behavior to spin fluctuation enhancement of the spin Hall effect arising from the strong spin-orbit interaction between the conduction electrons and the localized Fe moments. There is also a strong T-dependent enhancement of the effective spin-mixing conductance of the FeCoB/FePt interface that we similarly attribute to spin fluctuations in the FePt ferromagnetic transition region. The peak strength of the DL SOT indicates an exceptionally large spin Hall angle, >0.34 near the Curie point of the FePt alloys. We also realized current-induced magnetization switching by the DL SOT in close vicinity to the Curie point of these ferromagnetic FePt alloys and measured the spin diffusion length to be quite similar, ≈ 1.5 nm, both above and in close vicinity to T_c. This fluctuation enhanced spin Hall effect, which is tunable through the composition of the FePt alloy, provides new opportunities for the study of spin-dependent scattering and transport in systems with very strong spin-orbit interactions, and for applications where a very strong spin current from a relatively low resistivity material can be particularly beneficial.

Y. O. thanks Shengjie Shi for the assistance in low temperature flip-chip FMR measurements. This research was supported by ONR (N000014-15-1-2449) and by NSF/MRSEC (DMR-1120296) through the Cornell Center for Materials Research (CCMR), and by NSF through use of the Cornell NanoScale Facility, an NNCI member (ECCS-1542081). The authors hold patents and have patent applications filed on their behalf regarding some aspects of the spin-orbit torque research discussed in this report.

*yo84@cornell.edu
†rab8@cornell.edu.

[1] I. M. Miron, G. Gaudin, S. Auffret, B. Rodmacq, A. Schuhl, S. Pizzini, J. Vogel, and P. Gambardella, Nat. Mater. **9**, 230 (2010).
[2] I. M. Miron, K. Garello, G. Gaudin, P.-J. Zermatten, M. V. Costache, S. Auffret, S. Bandiera, B. Rodmacq, A. Schuhl, and P. Gambardella, Nature (London) **476**, 189 (2011).
[3] L. Liu, T. Moriyama, D. C. Ralph, and R. A. Buhrman, Phys. Rev. Lett. **106**, 036601 (2011).
[4] L. Liu, C.-F. Pai, Y. Li, H. W. Tseng, D. C. Ralph, and R. A. Buhrman, Science **336**, 555 (2012).
[5] C.-F. Pai, L. Liu, Y. Li, H. W. Tseng, D. C. Ralph, and R. A. Buhrman, Appl. Phys. Lett. **101**, 122404 (2012).
[6] N. Reynolds, P. Jadaun, J. T. Heron, C. L. Jermain, J. Gibbons, R. Collette, R. A. Buhrman, D. G. Schlom, and D. C. Ralph, Phys. Rev. B **95**, 064412 (2017).
[7] S. Emori, U. Bauer, S.-M. Ahn, E. Martinez, and G. S. D. Beach, Nat. Mater. **12**, 611 (2013).
[8] W. Jiang, P. Upadhyaya, W. Zhang, G. Yu, M. B. Jungfleisch, F. Y. Fradin, J. E. Pearson, Y. Tserkovnyak, K. L. Wang, O. Heinonen, S. G. E. te Velthuis, and A. Hoffmann, Science **349**, 283 (2015).
[9] A. Hoffmann, IEEE Trans. Magn. **49**, 5172 (2013).
[10] J. Sinova, S. O. Valenzuela, J. Wunderlich, C. H. Back, and T. Jungwirth, Rev. Mod. Phys. **87**, 1213 (2015).
[11] Y. Niimi, M. Morota, D. H. Wei, C. Deranlot, M. Basletic, A. Hamzic, A. Fert, and Y. Otani, Phys. Rev. Lett. **106**, 126601 (2011).
[12] M. Yamanouchi, L. Chen, J. Kim, M. Hayashi, H. Sato, S. Fukami, S. Ikeda, F. Matsukura, and H. Ohno, Appl. Phys. Lett. **102**, 212408 (2013).
[13] Y. Niimi, Y. Kawanishi, D. H. Wei, C. Deranlot, H. X. Yang, M. Chshiev, T. Valet, A. Fert, and Y. Otani, Phys. Rev. Lett. **109**, 156602 (2012).
[14] M. Obstbaum, M. Decker, A. K. Greitner, M. Haertinger, T. N. G. Meier, M. Kronseder, K. Chadova, S. Wimmer, D. Kodderitzsch, H. Ebert, and C. H. Back, Phys. Rev. Lett. **117**, 167204 (2016).
[15] D. H. Wei, Y. Niimi, B. Gu, T. Ziman, S. Maekawa, and Y. Otani, Nat. Commun. **3**, 1058 (2012).
[16] J. Crangle and W. R. Scott, J. Appl. Phys. **36**, 921 (1965).
[17] J.-U. Thiele, L. Folks, M. F. Toney, and D. K. Weller, J. Appl. Phys. **84**, 5686 (1998).
[18] K. M. Seemann, Y. Mokrousov, A. Aziz, J. Miguel, F. Kronast, W. Kuch, M. G. Blamire, A. T. Hindmarch, B. J. Hickey, I. Souza, and C. H. Marrows, Phys. Rev. Lett. **104**, 076402 (2010).
[19] G. E. Bacon, A. E. R. E. Harwell, and J. Crangle, Proc. R. Soc. A **272**, 387 (1963).
[20] T. Saerbeck, H. Zhu, D. Lott, H. Lee, P. R. Leclair, G. J. Mankey, A. P. J. Stampfl, and F. Klose, J. Appl. Phys. **114**, 013901 (2013).

[21] G. X. Miao and G. Xiao, Appl. Phys. Lett. **85**, 73 (2004).
[22] J. Moritz, B. Rodmacq, S. Auffret, and B. Dieny, J. Phys. D **41**, 135001 (2008).
[23] T. Taniguchi, J. Grollier, and M. D. Stiles, Phys. Rev. Applied **3**, 044001 (2015).
[24] S. Maat, A. J. Kellock, D. Weller, J. E. E. Baglin, and E. E. Fullerton, J. Magn. Magn. Mater. **265**, 1 (2003).
[25] R. C. O'Handley, *Modern Magnetic Materials—Principles and Applications* (John Wiley & Sons, New York, 2000).
[26] K. Garello, I. M. Miron, C. O. Avci, F. Freimuth, Y. Mokrousov, S. Blügel, S. Auffret, O. Boulle, G. Gaudin, and P. Gambardella, Nat. Nanotechnol. **8**, 587 (2013).
[27] M. Hayashi, J. Kim, M. Yamanouchi, and H. Ohno, Phys. Rev. B **89**, 144425 (2014).
[28] W. Zhang, W. Han, X. Jiang, S.-H. Yang, and S. S. P. Parkin, Nat. Phys. **11**, 496 (2015).
[29] C.-F. Pai, Y. Ou, L. H. Vilela-Leão, D. C. Ralph, and R. A. Buhrman, Phys. Rev. B **92**, 064426 (2015).
[30] Y. Ou, D. C. Ralph, and R. A. Buhrman, Appl. Phys. Lett. **110**, 192403 (2017).
[31] See Supplemental Material at http://link.aps.org/supplemental/10.1103/PhysRevLett.120.097203 for more details regarding the AHE measurements, harmonic response measurements and FMR measurements at various temperatures.
[32] J. Kim, J. Sinha, S. Mitani, M. Hayashi, S. Takahashi, S. Maekawa, M. Yamanouchi, and H. Ohno, Phys. Rev. B **89**, 174424 (2014).
[33] Y. Ou, C.-F. Pai, S. Shi, D. C. Ralph, and R. A. Buhrman, Phys. Rev. B **94**, 140414 (2016).
[34] C.-F. Pai, M.-H. Nguyen, C. Belvin, L. H. Vilela-Leão, D. C. Ralph, and R. A. Buhrman, Appl. Phys. Lett. **104**, 082407 (2014).
[35] J. Kondo, Prog. Theor. Phys. **27**, 772 (1962).
[36] J. P. Jan, Helv. Phys. Acta **25**, 677 (1952).
[37] B. Gu, T. Ziman, and S. Maekawa, Phys. Rev. B **86**, 241303 (2012).
[38] Y. Ohnuma, H. Adachi, E. Saitoh, and S. Maekawa, Phys. Rev. B **89**, 174417 (2014).
[39] Z. Qiu, J. Li, D. Hou, E. Arenholz, A. T. NDiaye, A. Tan, K. Uchida, K. Sato, S. Okamoto, Y. Tserkovnyak, Z. Q. Qiu, and E. Saitoh, Nat. Commun. **7**, 12670 (2016).
[40] L. Frangou, S. Oyarzún, S. Auffret, L. Vila, S. Gambarelli, and V. Baltz, Phys. Rev. Lett. **116**, 077203 (2016).
[41] Y. Tserkovnyak, A. Brataas, and G. E. W. Bauer, Phys. Rev. B **66**, 224403 (2002).
[42] F. D. Czeschka, L. Dreher, M. S. Brandt, M. Weiler, M. Althammer, I.-M. Imort, G. Reiss, A. Thomas, W. Schoch, W. Limmer, H. Huebl, R. Gross, and S. T. B. Goennenwein, Phys. Rev. Lett. **107**, 046601 (2011).
[43] P. M. Haney, H.-W. Lee, K.-J. Lee, A. Manchon, and M. D. Stiles, Phys. Rev. B **87**, 174411 (2013).
[44] L. Liu, O. J. Lee, T. J. Gudmundsen, D. C. Ralph, and R. A. Buhrman, Phys. Rev. Lett. **109**, 096602 (2012).